Supplementary information

Revealing Energy Transfer Mechanisms and Accelerating Intelligent Detection: Cr^{3+} and Ni^{2+} Co-Doped $Lu_2CaMg_2Si_3O_{12}$ Phosphors for NIR Applications

Zaidong Chen,[a] Yuefei Xiang,[a] Xinghui Qin,[a] Lei Zhong,[a] Hong Liao,[b] Shiwen Liu,[a] Jiaqi Wang,[a] Kezhi Zheng,[b] Dejian Hou,[c] Lei Zhou *[a] and Mingmei Wu [a]

[a.] Zhuhai Key Laboratory of Optoelectronic Functional Materials and Membrane Technology/School of Chemical Engineering and Technology/School of Marine Sciences, Sun Yat-sen University, Zhuhai, 519082, P. R. China.

[b.] School of Physics, South China Normal University, Guangzhou, 510006, P. R. China.

[c.] School of Materials Science and Engineering, Hanshan Normal University, Chaozhou, Guangdong, 521041, P. R. China.

[*] Corresponding authors: Lei Zhou

E-mail: zhoul8@mail.sysu.edu.cn

Results and Discussion

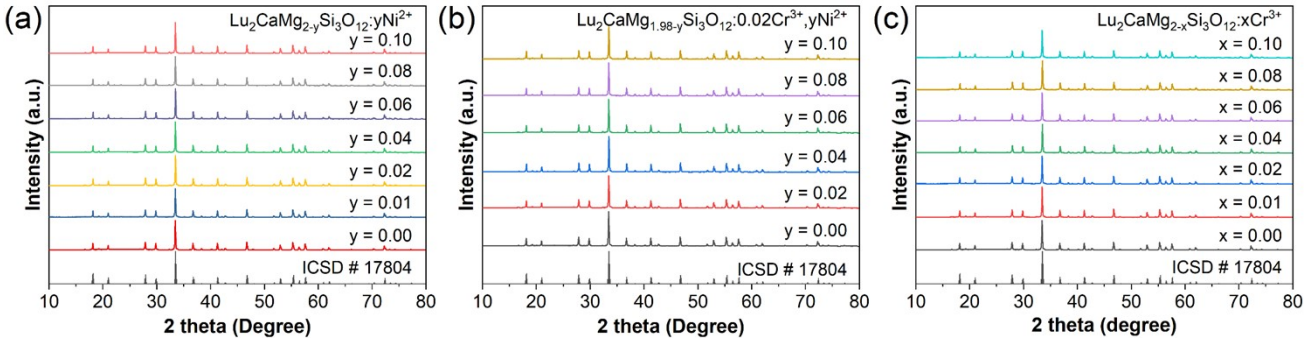

Fig. S1 XRD patterns of (a) $Lu_2CaMg_{2-y}Si_3O_{12}$:yNi^{2+}; (b) $Lu_2CaMg_{1.98-y}Si_3O_{12}$:$0.02Cr^{3+}$,$yNi^{2+}$, and (c) $Lu_2CaMg_{2-x}Si_3O_{12}$:xCr^{3+}.

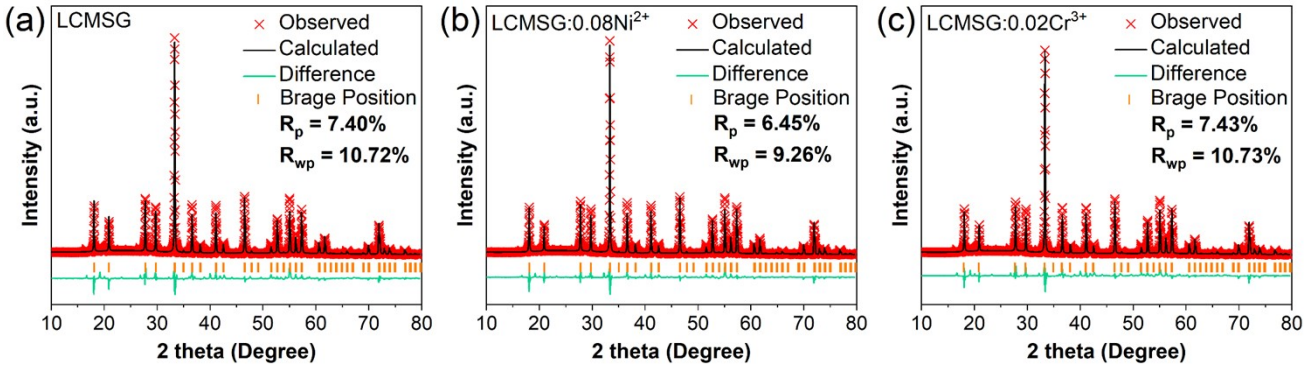

Fig. S2 Rietveld refinements for XRD patterns. (a) $Lu_2CaMg_2Si_3O_{12}$ host; (b) $Lu_2CaMg_{1.92}Si_3O_{12}$:$0.08Ni^{2+}$; (c) $Lu_2CaMg_{1.98}Si_3O_{12}$:$0.02Cr^{3+}$.

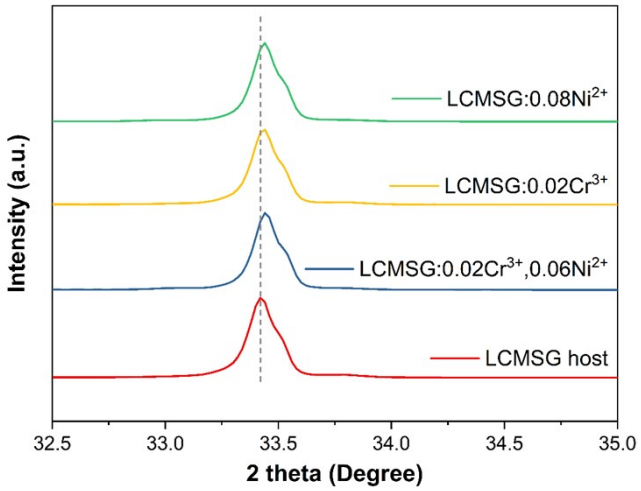

Fig. S3 The partial magnification of XRD patterns for $Lu_2CaMg_2Si_3O_{12}$ host, $Lu_2CaMg_{1.92}Si_3O_{12}$:$0.08Ni^{2+}$, $Lu_2CaMg_{1.98}Si_3O_{12}$:$0.02Cr^{3+}$, and $Lu_2CaMg_{1.92}Si_3O_{12}$: $0.02Cr^{3+}$,$0.06Ni^{2+}$.

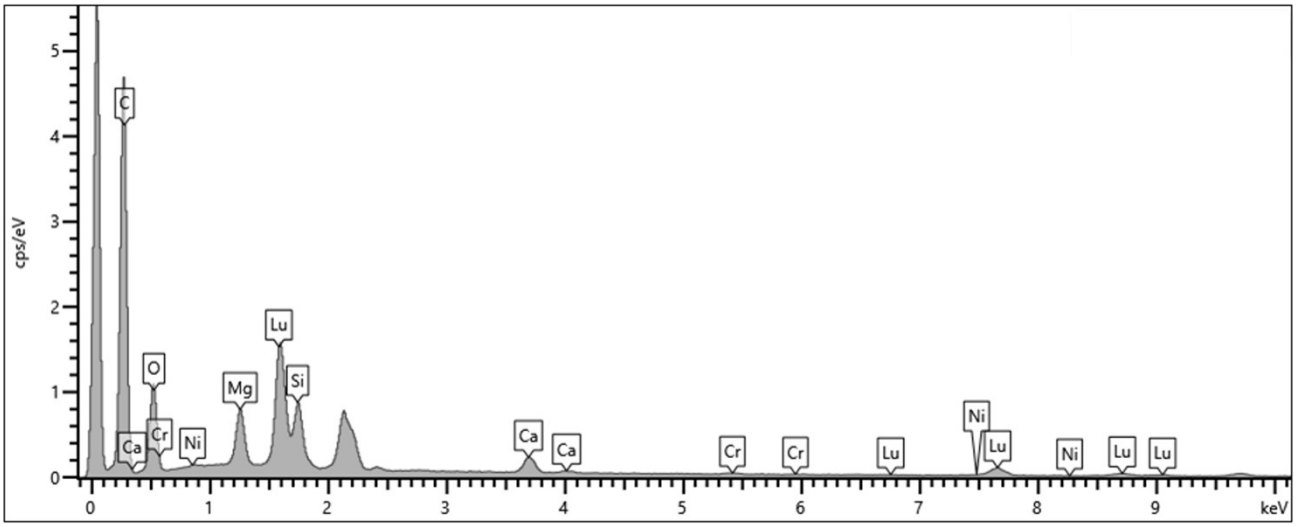

Fig. S4 EDS of $Lu_2CaMg_{1.84}Si_3O_{12}$:0.08$Cr^{3+}$,0.08$Ni^{2+}$.

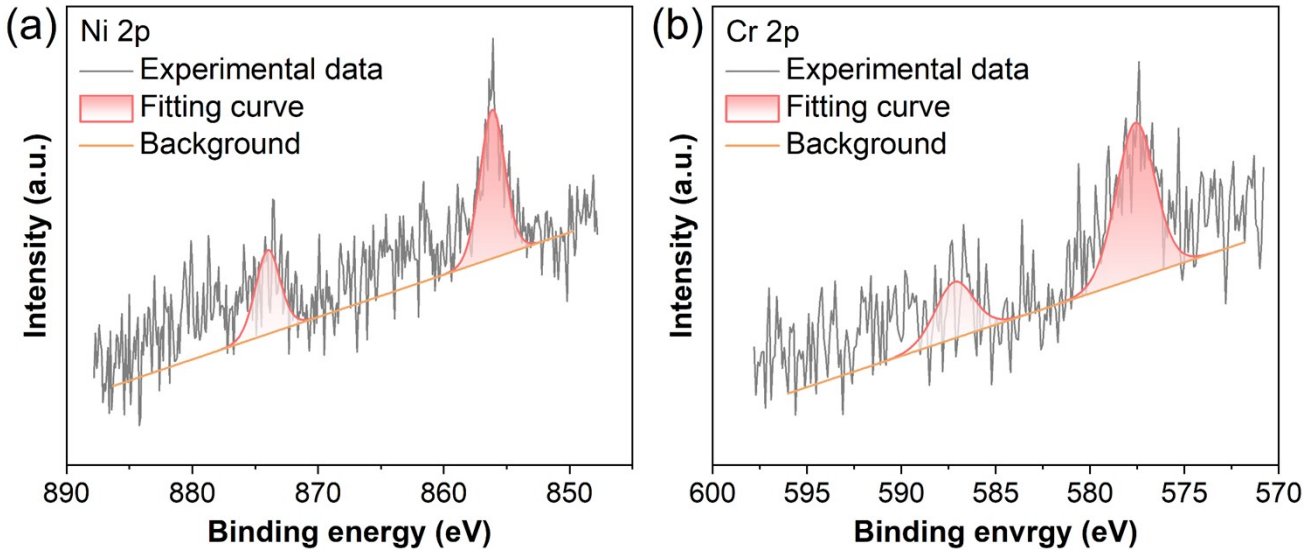

Fig. S5 XPS fine spectra of $Lu_2CaMg_{1.84}Si_3O_{12}$:0.08$Cr^{3+}$,0.08$Ni^{2+}$: (a) Ni 2p; (b) Cr 2p.

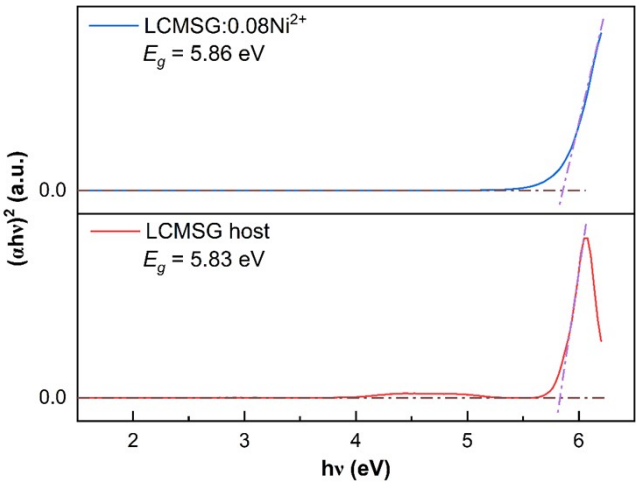

Fig. S6 Experimental determination E_g of $Lu_2CaMg_2Si_3O_{12}$ host and $Lu_2CaMg_{1.92}Si_3O_{12}$:0.08$Ni^{2+}$.

Based on DRS data, the absorbance data can be obtained using Kubelka-Munk formula[1]:

$$F(R) = (1 - R)^2/(2R) = K/S \qquad \text{(S1)}$$

Where R stands for reflectance, K and S represent absorption coefficient and scattering coefficient.

The energy band gap (E_g) could be evaluated using Tauc relation[2]:

$$[F(R)hv]^{1/n} = A(hv - E_g) \qquad \text{(S2)}$$

Where hv and A stand for photon energy and absorption constant, respectively. The n values of 1/2 and 2 correspond to direct and indirect allowed transitions in the same order. The electronic transition of $Lu_2CaMg_2Si_3O_{12}$ in this work belongs to direct allowed transition (n = 1/2). The band gap of the $Lu_2CaMg_2Si_3O_{12}$ host and the $Lu_2CaMg_{1.92}Si_3O_{12}$:0.08$Ni^{2+}$ samples are 5.83 and 5.86 eV, respectively.

The luminescence decay curves of $Lu_2CaMg_{2-y}Si_3O_{12}$:$y$$Ni^{2+}$ can be conformed to the double exponential function as described in equation (S3):

$$I = A_1 \exp\left(\frac{t}{\tau_1}\right) - A_2\, exp(\frac{t}{\tau_2}) \qquad \text{(S3)}$$

Where A_1 and A_2 are constants, I represents the luminescence intensity, t is time, τ_1 and τ_2 correspond to the lifetimes of the two exponential components.

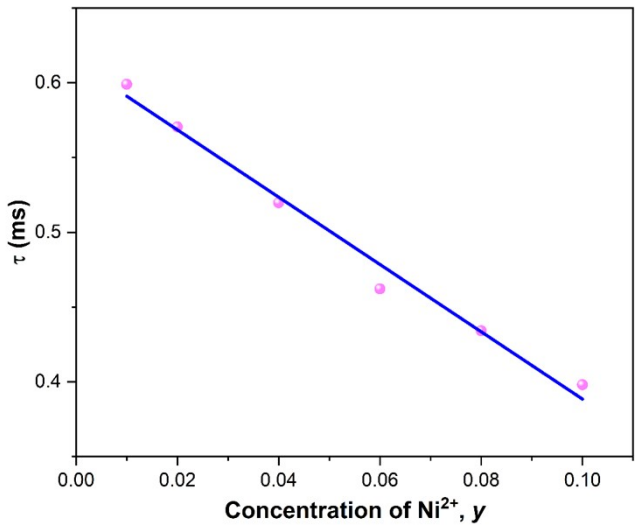

Fig. S7 Variation of $Lu_2CaMg_{2-y}Si_3O_{12}$:$y$$Ni^{2+}$ decay lifetime with Ni^{2+} concentration, y.

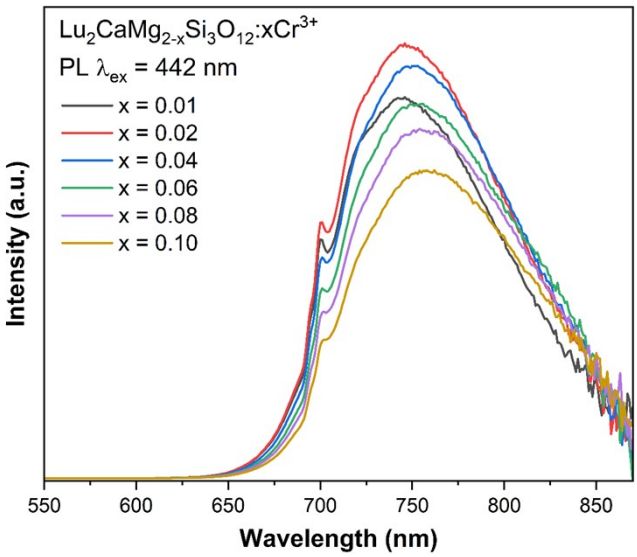

Fig. S8 PL spectra of $Lu_2CaMg_{2-x}Si_3O_{12}$:$x$$Cr^{3+}$.

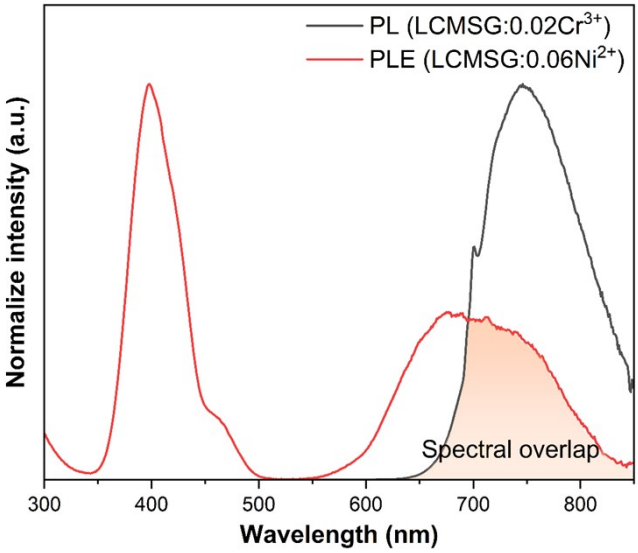

Fig. S9 Spectral overlap between PL of Cr^{3+} and PLE of Ni^{2+}.

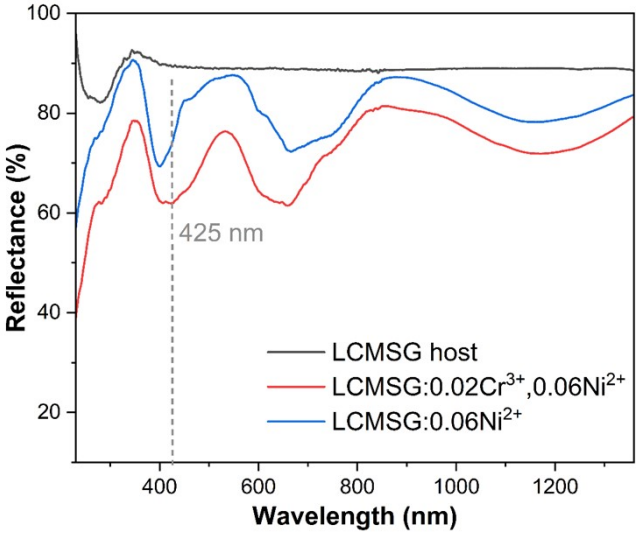

Fig. S10 The DRS of the $Lu_2CaMg_2Si_3O_{12}$ host, $Lu_2CaMg_{1.92}Si_3O_{12}$:0.02$Cr^{3+}$,0.06$Ni^{2+}$ samples and $Lu_2CaMg_{1.94}Si_3O_{12}$:0.06$Ni^{2+}$ samples.

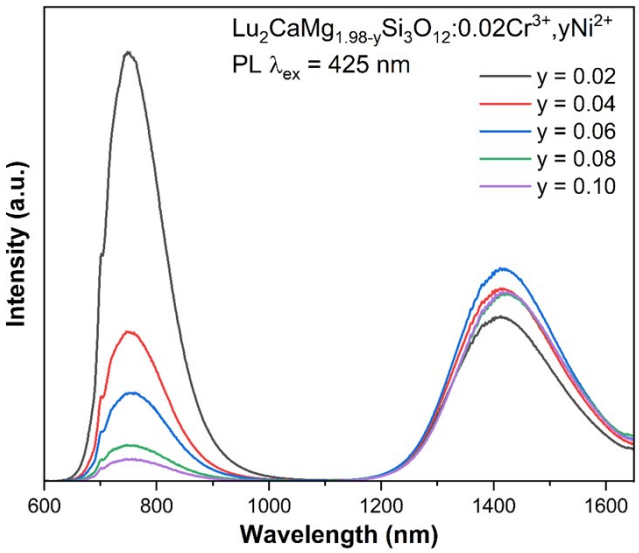

Fig. S11 PL spectra of $Lu_2CaMg_{1.98-y}Si_3O_{12}$:0.02$Cr^{3+}$,y$Ni^{2+}$ phosphors upon 425 nm excitation.

Dexter's method to calculate R_0 (Fig. S12a to Fig. S12h):[3]

(a) Measure the emission spectrum of $Lu_2CaMg_{1.98}Si_3O_{12}$:0.02$Cr^{3+}$ and calculate emission area by integration: 1.8223×10^9.

(b) Convert the emission spectrum of $Lu_2CaMg_{1.98}Si_3O_{12}$:0.02$Cr^{3+}$ into energy coordinates. $I(E) = I(\lambda)\lambda^2$: $y(b) = y(a) \times \lambda^2$. $x(b) = 1239.84 \div x(a)$. Calculate emission area by integration: 2.2594×10^{12}.

(c) Normalize the area of the emission spectrum of $Lu_2CaMg_{1.98}Si_3O_{12}$:0.02$Cr^{3+}$ by dividing: $y(c) = y(b) \div (2.2594 \times 10^{12})$.

(d) Measure the excitation spectrum of $Lu_2CaMg_{1.94}Si_3O_{12}$:0.06$Ni^{2+}$.

(e) Convert the ordinate of $Lu_2CaMg_{1.94}Si_3O_{12}$:0.06$Ni^{2+}$ to absorption cross section σ and the abscissa to energy: $\sigma(e) = (\ln 10 \times 1000/L) \times y(d)$; $x(e) = 1239.84 \div x(d)$. Where L is Avogadro number and σ is in cm^2. Calculate area of σ by integration: 1.1468 × 10^{-16}. $\int \sigma(E)dE = Q_A$; So Q_A = 1.1468 × 10^{-16} cm^2 eV^{-1}. Where Q_A is the absorption cross-section of the acceptor.

(f) Normalize the area of the absorption cross section (σ) of $Lu_2CaMg_{1.94}Si_3O_{12}$:0.06$Ni^{2+}$ by dividing: $y(f) = y(e) \div (1.1468 \times 10^{-16})$.

(g) Overlap the normalized emission of $Lu_2CaMg_{1.98}Si_3O_{12}$:0.02$Cr^{3+}$ and absorption cross section σ of $Lu_2CaMg_{1.94}Si_3O_{12}$:0.06$Ni^{2+}$.

(h) Calculating the summation $\int f_D(E)f_A(E)E^{-4}dE$, as follow: $y(h) = y(c)[i] \times y(f)[i] \times (x[i+1] - x[i])/x[i]^4$. The result of $\int f_D(E)f_A(E)E^{-4}dE$ in this work is 4.6646 × 10^{-4}. Where $[i]$ is the rows, as shown in Fig. S12h.

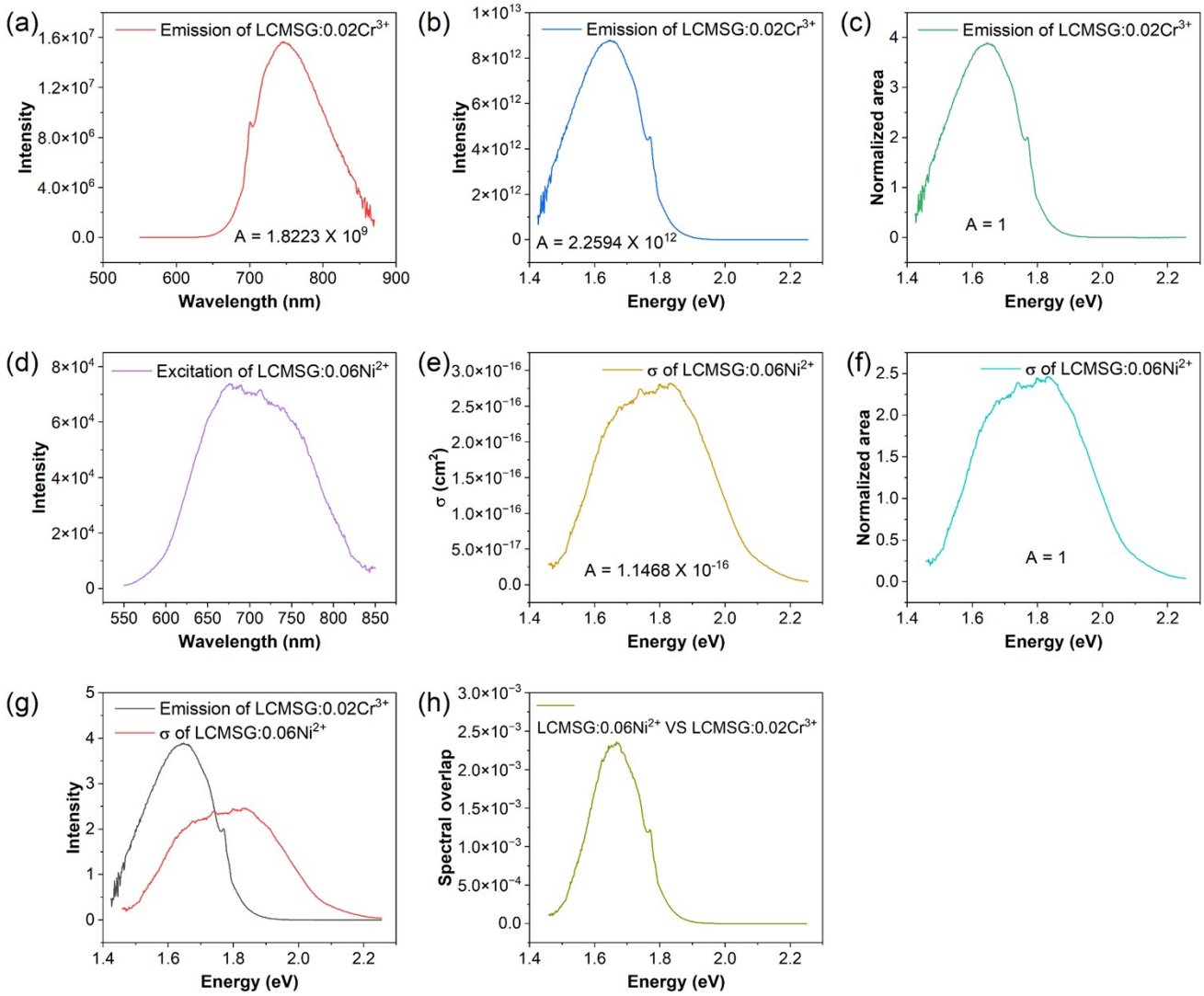

Fig. S12 Dexter's method to calculate R_0: (a) Emission spectrum of $Lu_2CaMg_{1.98}Si_3O_{12}:0.02Cr^{3+}$; (b) Energy coordinates emission spectrum of $Lu_2CaMg_{1.98}Si_3O_{12}:0.02Cr^{3+}$; (c) Normalized emission area of $Lu_2CaMg_{1.98}Si_3O_{12}:0.02Cr^{3+}$; (d) Excitation spectrum of $Lu_2CaMg_{1.94}Si_3O_{12}:0.06Ni^{2+}$; (e) Absorption cross-section of $Lu_2CaMg_{1.94}Si_3O_{12}:0.06Ni^{2+}$; (f) Normalized absorption cross-section of $Lu_2CaMg_{1.94}Si_3O_{12}:0.06Ni^{2+}$; (g) Normalized absorption cross-section of $Lu_2CaMg_{1.94}Si_3O_{12}:0.06Ni^{2+}$ and normalized emission spectrum of $Lu_2CaMg_{1.98}Si_3O_{12}:0.02Cr^{3+}$; (h) Spectral overlap of $Lu_2CaMg_{1.94}Si_3O_{12}:0.06Ni^{2+}$ and $Lu_2CaMg_{1.98}Si_3O_{12}:0.02Cr^{3+}$.

Temperature sensing performance

Fig. S13a illustrates the luminescence properties of $Lu_2CaMg_{1.92}Si_3O_{12}$:0.02$Cr^{3+}$,0.06$Ni^{2+}$ after three cycles of low-high-low temperature, demonstrating minimal changes in luminescence intensity. This observation highlights the excellent temperature repeatability of the $Lu_2CaMg_{1.92}Si_3O_{12}$:0.02$Cr^{3+}$,0.06$Ni^{2+}$ phosphor across the 123 to 448 K range. Notably, the luminescence intensity of Ni^{2+} decreases more rapidly than that of Cr^{3+} as the temperature increases (Fig. S13b), indicating that the $Lu_2CaMg_{1.92}Si_3O_{12}$:0.02$Cr^{3+}$,0.06$Ni^{2+}$ phosphor is suitable for dual-mode optical thermometry. The potential dual-mode optical thermometry, based on the fluorescence intensity ratio (FIR), is expressed in the following equation:[4]

$$FIR = \frac{I_{Cr^{3+}}}{I_{Ni^{2+}}} = A + B\,exp(-\Delta E/(k_B T)) \quad \text{(S4)}$$

Where A, B are constants, ΔE is the energy gap, k_B is the Boltzmann's constant, and T is the Kelvin temperature. As shown in Fig. S13c, the measured plots of FIR can be well fitted by equation (S4), confirming the phosphor's suitability for dual-mode optical thermometry. To further evaluate the optical thermometry performance of this phosphor, it is necessary to investigate the absolute sensitivity (S_a) and relative sensitivity (S_r), which are expressed by the equations (S5) and (S6):[5]

$$S_a = \left|\frac{\partial FIR}{\partial T}\right| = B\exp\left(-\Delta E/(k_B T)\right) \times \frac{\Delta E}{k_B T^2} \quad \text{(S5)}$$

$$S_r = \left|\frac{1}{FIR}\frac{\partial FIR}{\partial T}\right| \times 100\% = \frac{B\exp\left(-\Delta E/(k_B T)\right)}{A + B\exp\left(-\Delta E/(k_B T)\right)} \times \frac{\Delta E}{k_B T^2} \times 100\% \quad \text{(S6)}$$

The maximum S_a value is 1.01×10^{-3} K^{-1} at 448 K and the maximum S_r is 0.42% K^{-1} at 298 K, as presented in Fig. S13d. Table S3 lists some reported candidate materials for optical thermometry. The above results indicate that this phosphor has potential for application in optical thermometry.

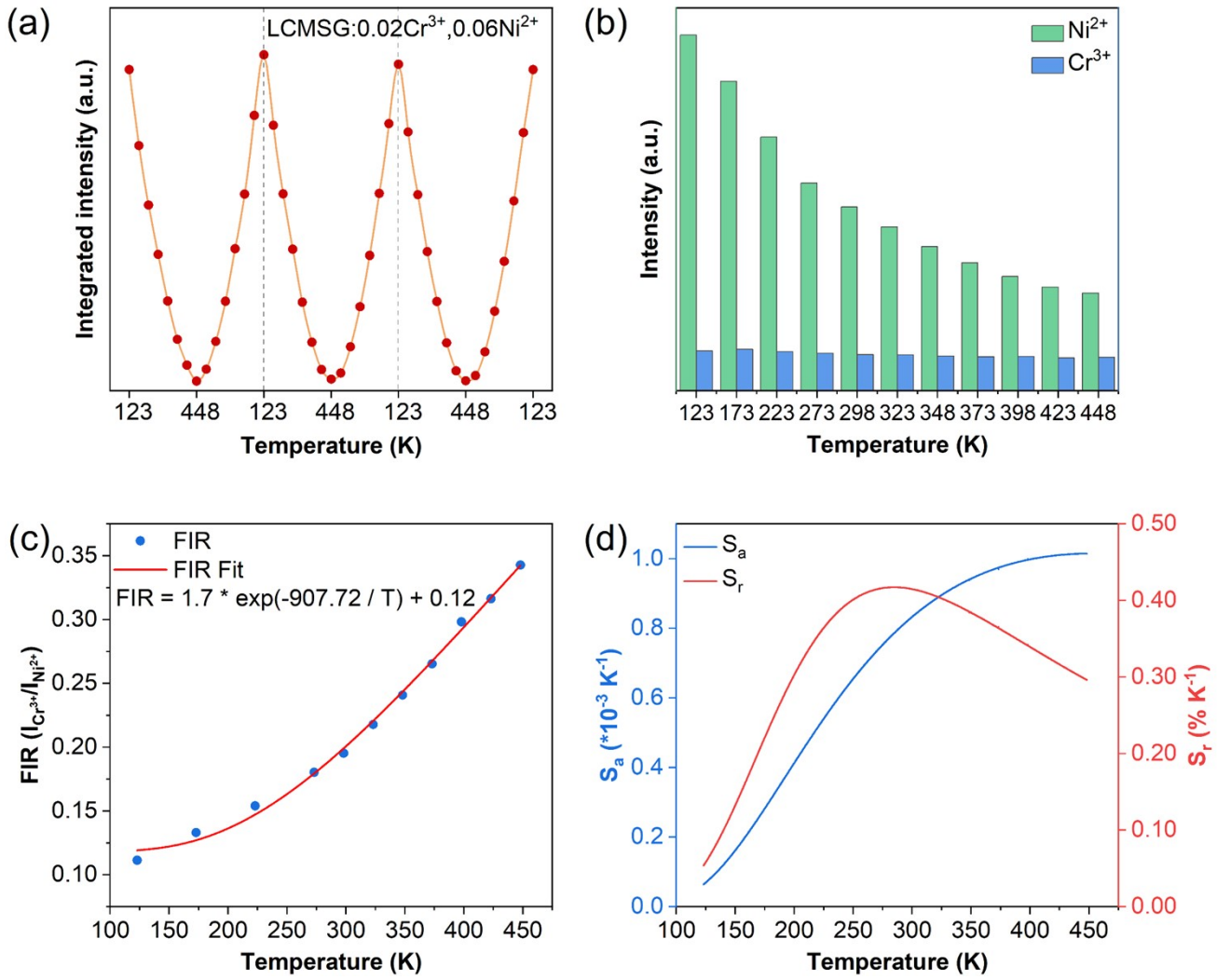

Fig. S13 (a) Temperature cycle stability of the $Lu_2CaMg_{1.92}Si_3O_{12}$:0.02$Cr^{3+}$,0.06$Ni^{2+}$ sample; (b) Emission intensity of Cr^{3+} and Ni^{2+} at various temperatures; (c) FIR plots and the fitting curve of $Lu_2CaMg_{1.92}Si_3O_{12}$:0.02$Cr^{3+}$,0.06$Ni^{2+}$; (d) Absolute sensitivity S_a and relative sensitivity S_r of $Lu_2CaMg_{1.92}Si_3O_{12}$:0.02$Cr^{3+}$,0.06$Ni^{2+}$.

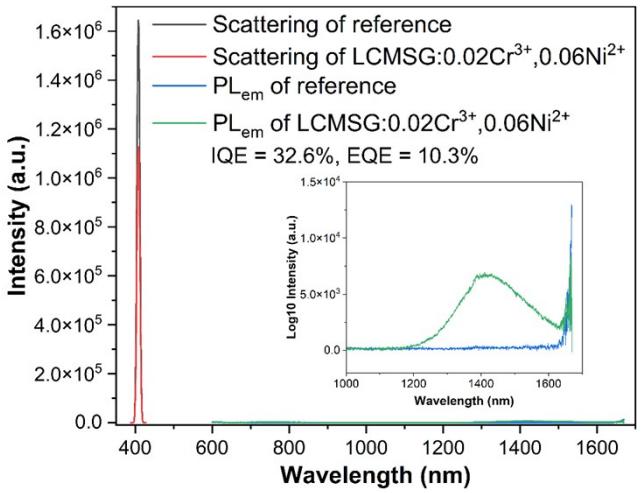

Fig. S14 IQE and EQE of $Lu_2CaMg_{1.92}Si_3O_{12}$:0.02$Cr^{3+}$,0.06$Ni^{2+}$ at RT.

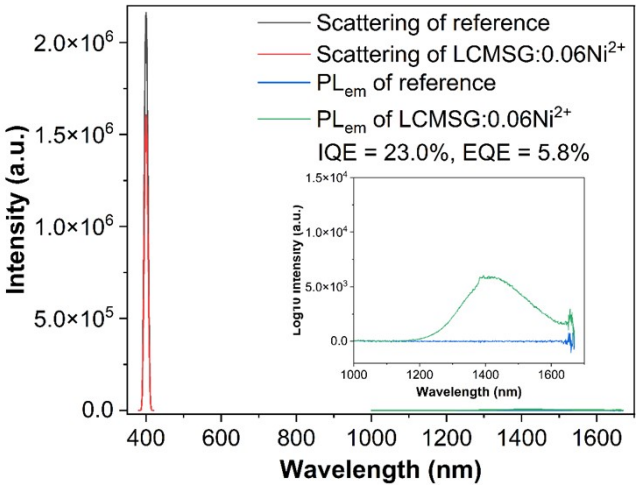

Fig. S15 IQE and EQE of $Lu_2CaMg_{1.94}Si_3O_{12}$:0.06$Ni^{2+}$ at RT.

Table S1. Rietveld refinement results of $Lu_2CaMg_2Si_3O_{12}$ host, $Lu_2CaMg_{1.98}Si_3O_{12}$:0.02$Cr^{3+}$, $Lu_2CaMg_{1.92}Si_3O_{12}$:0.08$Ni^{2+}$, and $Lu_2CaMg_{1.92}Si_3O_{12}$:0.02$Cr^{3+}$,0.06$Ni^{2+}$.

	host	**0.02Cr^{3+}**	**0.08Ni^{2+}**	**0.02Cr^{3+},0.06Ni^{2+}**
Space group	Ia-3d	Ia-3d	Ia-3d	Ia-3d
***a* = *b* = *c* (Å)**	12.02219	12.01892	12.02394	12.02509
***α* = *β* = *γ* (°)**	90	90	90	90
Cell volume (Å^3)	1737.6022	1736.1875	1738.3644	1738.8604
R_p (%)	7.40	7.43	6.45	6.37
R_{wp} (%)	10.72	10.73	9.26	9.21

Table S2. Theoretical and experimental ratios of elements in $Lu_2CaMg_{1.84}Si_3O_{12}$:0.08$Cr^{3+}$,0.08$Ni^{2+}$ based on EDS results.

EDS	**Lu**	**Ca**	**Mg**	**Si**	**O**	**Cr**	**Ni**
Theoretical mass ratio	48.61	5.57	6.21	11.71	26.67	0.58	0.65
Theoretical atomic ratio	2.00	1.00	1.84	3.00	12.00	0.08	0.08
Experimental mass ratio	45.10	5.70	6.49	12.41	28.70	1.15	0.45
Experimental atomic ratio	1.85	1.02	1.92	3.18	12.91	0.16	0.06

Table S3. Optical thermometry properties of several reported NIR phosphors.

Phosphors	Temperature (K)	S_r (% K^{-1})	Refs
$Y_3Al_5O_{12}:Cr^{3+}$	123-563	0.52	6
$LiGa_5O_8:Cr^{3+}$	300-463	0.59	7
$Gd_2GaSb_{0.9}Ta_{0.1}O_7:Cr^{3+},Yb^{3+}$	303-573	0.60	8
$LiLaP_4O_{12}:Cr^{3+},Yb^{3+}$	77-550	0.32	9
$ZnGa_2O_4:Bi^{3+},Cr^{3+}$	293-473	0.31	10
$BaAl_{12}O_{19}:Eu^{2+},Cr^{3+}$	293-563	0.466	11
$SrTiO_3:Ni^{2+},Er^{3+}$	183-473	0.44	12
$LaZnGa_{11}O_{19}:Cr^{3+},Ni^{2+}$	100-450	0.61	13
$Mg_3Ga_2GeO_8:Cr^{3+},Ni^{2+}$	275-475	0.55	14
$Lu_2CaMg_2Si_3O_{12}:Cr^{3+},Ni^{2+}$	123-448	0.42	This work

References

1 P. Kubelka and F. Munk, *Z. Tech. Phys.,* 1931, **12**, 593-601.

2 J. Tauc, A. Menth and D. L. Wood, *Phys. Rev. Lett.*, 1970, **25**, 749-752.

3 P. A. Tanner, L. Zhou, C. Duan and K.-L. Wong, *Chem. Soc. Rev.*, 2018, **47**, 5234-5265.

4 Y. Gao, F. Huang, H. Lin, J. Zhou, J. Xu and Y. Wang, *Adv. Funct. Mater.*, 2016, **26**, 3139-3145.

5 M. D. Dramićanin, Ł. Marciniak, S. Kuzman, W. Piotrowski, Z. Ristić, J. Periša, I. Evans, J. Mitrić, V. Đorđević, N. Romčević, M. G. Brik and C. G. Ma, *Light: Sci. Appl.*, 2022, **11**, 279.

6 A. Zabiliūtė, S. Butkutė, A. Žukauskas, P. Vitta and A. Kareiva, *Appl. Opt,*, 2014, **53**, 907-914.

7 D. Chen, Z. Wan and Y. Zhou, *Opt. Lett.*, 2015, **40**, 3607,3610.

8 L. Ma, R. Wei, Q. Yu, P. Dai, X. Tian, F. Hu and H. Guo, *Mater. Today Chem.*, 2024, **38**, 102090.

9 L. Marciniak and A. Bednarkiewicz, *Sens. Actuators B: Chem.*, 2017, **243**, 388-393.

10 E. Glais, M. Pellerin, V. Castaing, D. Alloyeau, N. Touati, B. Viana and C. Chanéac, *RSC. Adv.*, 2018, **8**, 41767-41774.

11 Y. Zhu, C. Li, D. Deng, H. Yu, H. Li, L. Wang, C. Shen, X. Jing and S. Xu, *J. Lumin.*, 2021, **237**, 118142.

12 C. Matuszewska and L. Marciniak, *J. Lumin.*, 2020, **223**, 117221.

13 Q. Zhang, G. Li, G. Li, D. Liu, P. Dang, L. Qiu, H. Lian, M. S. Molokeev and J. Lin, *Adv. Opt. Mater.*, 2024, **12**, 2301429.

14 C. Wang, Y. Niu, Y. Wang, F. Wu, Q. Zhang, Y. Teng, H. Dong and Z. Mu, *Inorg. Chem.*, 2024, **63**, 14383-14391.